PHILOSOPHICAL TRANSACTIONS OF THE ROYAL SOCIETY A MATHEMATICAL, PHYSICAL & ENGINEERING SCIENCES

A simple pendulum laser interferometer for determining the gravitational constant

Harold V. Parks and James E. Faller

Phil. Trans. R. Soc. A 2014 **372**, 20140024, published 8 September 2014

PHILOSOPHICAL TRANSACTIONS OF THE ROYAL SOCIETY A

rsta.royalsocietypublishing.org

Research

Cite this article: Parks HV, Faller JE. 2014 A simple pendulum laser interferometer for determining the gravitational constant. *Phil. Trans. R. Soc. A* **372**: 20140024.
http://dx.doi.org/10.1098/rsta.2014.0024

One contribution of 13 to a Theo Murphy Meeting Issue 'The Newtonian constant of gravitation, a constant too difficult to measure?'

Subject Areas:
mechanics

Keywords:
gravitational constant, Fabry–Perot interfometer, precision measurement, physical constants

Author for correspondence:
Harold V. Parks
e-mail: harold.parks@nrc-cnrc.gc.ca

†Present address: National Research Council of Canada, Ottawa, ON K1A 0R6, Canada.

Royal Society Publishing

A simple pendulum laser interferometer for determining the gravitational constant

Harold V. Parks[1,2,†] and James E. Faller[1,3]

[1]JILA, University of Colorado and National Institute of Standards and Technology, Boulder, CO 80309, USA
[2]Sandia National Laboratories, Albuquerque, NM 87185, USA
[3]Institute for Gravitational Research, School of Physics and Astronomy, University of Glasgow, Glasgow G12 8QQ, UK

We present a detailed account of our 2004 experiment to measure the Newtonian constant of gravitation with a suspended laser interferometer. The apparatus consists of two simple pendulums hanging from a common support. Each pendulum has a length of 72 cm and their separation is 34 cm. A mirror is embedded in each pendulum bob, which then in combination form a Fabry–Perot cavity. A laser locked to the cavity measures the change in pendulum separation as the gravitational field is modulated due to the displacement of four 120 kg tungsten masses.

1. Introduction

In 2004, we conducted an experiment at the University of Colorado in Boulder to measure the Newtonian constant of gravitation G [1], and we present here a description of the experiment expanded beyond that in the original publication. We obtained a value of $(6.672\,34 \pm 0.000\,14) \times 10^{-11}\ \mathrm{m^3\,kg^{-1}\,s^{-2}}$, which is below some recent measurements of G [2] but agrees with some older determinations [3]. Our experimental design is similar to the microwave interferometer constructed at the University of Wuppertal for determining G [4–6], but we replace the microwave interferometer with a laser interferometer. In addition, our source mass design allows us to reduce the uncertainties due to the positioning of the masses and floor tilt effects.

2. Overview of the apparatus

A schematic of the apparatus is shown in figure 1. Two 780 g copper pendulum bobs are each suspended by four wires so that the bobs translate without rotation and are constrained to move along one axis.

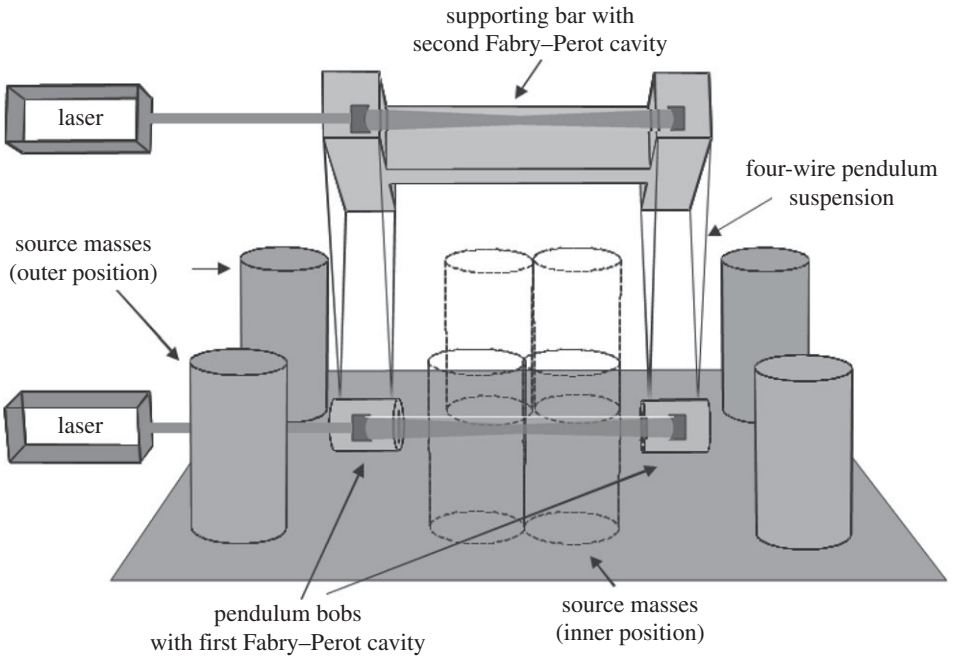

Figure 1. A schematic of the apparatus (not to scale). When the source masses are moved from the inner to the outer position, the change in the gravitational field causes the pendulum bob separation to change. This displacement is measured by beating a laser locked to a Fabry–Perot cavity formed from mirrors embedded in the pendulum bobs with a second laser locked to a cavity in the pendulum support.

The pendulums are 72 cm long. Four 120 kg tungsten source mass stacks produce a gravitational field that deflects the pendulums from vertical. When the source masses are placed between the pendulums, the gravitational force pulls the pendulums together; and when the source masses are moved on air bearings to a position outside of the pendulums, the bobs are pulled apart. This causes a total change in pendulum separation of 90 nm. Mirrors are embedded in the pendulum bobs, which are used to form a free-hanging Fabry–Perot cavity. The gravity signal is measured by beating a He–Ne laser locked to the pendulum cavity resonant frequency against an identical laser locked to a Fabry–Perot cavity located in the pendulum support region. This removes most of the effect of thermal expansion of the pendulum supporting bar from the gravity signal.

Not shown in figure 1 are magnets below the pendulum bobs, which reduce the swinging of the pendulums through eddy current damping. In order to calculate the gravitational force on the pendulum bobs given the measured displacement, the magnets are removed and the pendulums are allowed to swing freely. The pendulum restoring force can then be calculated from the period of oscillation.

A photograph of the apparatus as it appeared just before it was completed is shown in figure 2. The pendulums are enclosed in an aluminium vacuum chamber, which is held at a pressure of 1.5×10^{-5} Torr with an ion pump. This vacuum chamber is supported by two wings, which allow the chamber to hang over, but not touch, the 10 cm thick aluminium plate that the source masses ride on. This ensures that any flexing of the source mass support plate as the source masses move is not transmitted to the pendulum apparatus. The source mass positions in the inner and outer locations are precisely located using stops that contact the source masses at two points at the level of the pendulum bobs.

3. Gravity data

Eleven data runs were taken on 7 days between 12 May 2004 and 6 June 2004, with a break in the data between 14 May 2004 and 3 June 2004, because the stepper motor used to move the source

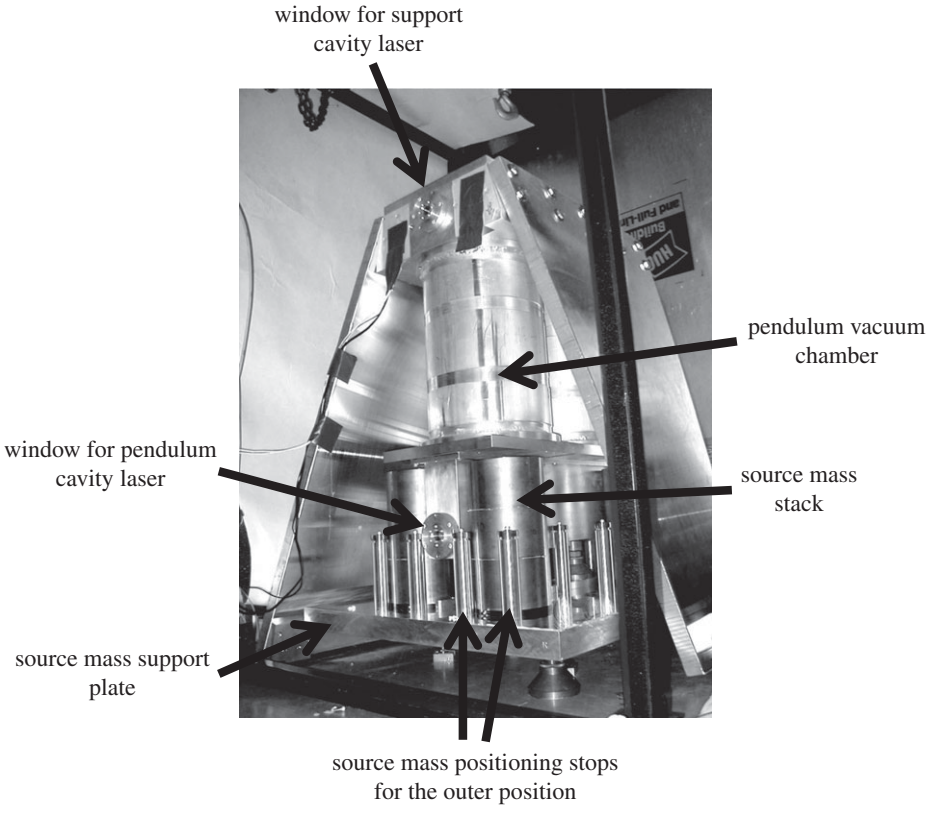

Figure 2. A photograph of the apparatus. The pendulums are enclosed in a vacuum chamber, and the windows for the top and bottom cavity lasers can be seen. The vacuum chamber hangs from two 'wing' plates that are bolted near the top of the chamber, so that it does not touch the source mass support palate. A source mass stack containing three tungsten billets can be seen. The stack float is on an air bearing and was positioned by moving against stops that contact the source mass stack half-way up. An insulated compartment was constructed around the apparatus to protect it from draughts.

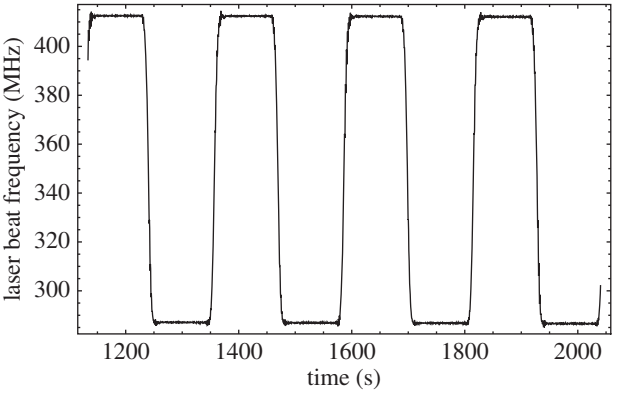

Figure 3. An example of the laser beat frequency signal as the source masses are moved between the inner and outer positions, changing the gravitational pull on the pendulum bobs. The 125 MHz signal corresponds to a change in pendulum bob separation of 90 nm.

masses failed. Each run consisted of between 1.5 and 7 h of continuous data. Runs were taken mostly at night when the sources of man-made vibration were the quietest. It was also observed that a nearby elevator added noise, perhaps through magnetic field fluctuations that induced eddy current in the bobs.

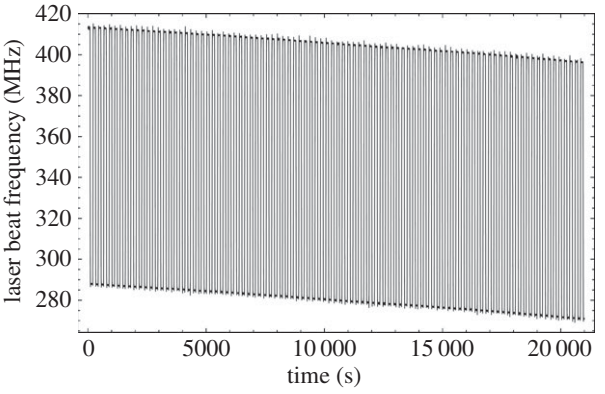

Figure 4. A longer section of data from the set shown in figure 3. A slow drift in the pendulum displacement can be seen. This drift is consistent with 5–10 μrad change in floor tilt that is observed in the laboratory over the course of a day coupling into the signal due to the slight difference in the lengths of the two pendulums.

Table 1. The *G* value plotted in figure 5 along with the raw laser beat frequency differences for each dataset. The set-to-set variation in the laser signal does not exactly correspond to variations in the *G* value because the source mass position was re-measured each day. In particular, there was a large change in position between 15 May and 2 June. The shading indicates where the positions were recalculated, with adjacent rows with the same shade assumed to have identical source mass positions. The uncertainties in the laser frequency listed here are based only on the scatter of the data within each set.

date	laser signal (MHz)	G ($\times 10^{-11}$ m^3 kg^{-1} s^{-2})
12 May 2004	125.3925 ± 0.0013	6.67235 ± 0.00012
12 May 2004	125.3916 ± 0.0014	6.67236 ± 0.00012
13 May 2004	125.3901 ± 0.0011	6.67228 ± 0.00011
14 May 2004	125.3895 ± 0.0013	6.67237 ± 0.00012
2 June 2004	125.4254 ± 0.0020	6.67242 ± 0.00014
3 June 2004	125.4265 ± 0.0008	6.67248 ± 0.00010
4 June 2004	125.4327 ± 0.0009	6.67236 ± 0.00011
4 June 2004	125.4306 ± 0.0011	6.67225 ± 0.00011
5 June 2004	125.4309 ± 0.0017	6.67226 ± 0.00013
5 June 2004	125.4360 ± 0.0013	6.67246 ± 0.00012
5 June 2004	125.4319 ± 0.0014	6.67223 ± 0.00011
6 June 2004	125.4345 ± 0.0007	6.67238 ± 0.00010
6 June 2004	125.4305 ± 0.0016	6.67224 ± 0.00013

A sample of the data from the interferometer is shown in figures 3 and 4. The source masses are held in one position for 80 s and then moved to the other position with a transit time of 35 s. The first 20 s of data after the source masses stop is dropped when computing the displacements. The 90 nm change in the interferometer cavity length due to the gravitational signal corresponds to a 125 MHz change in the cavity resonant frequency. The value of G is calculated from the displacement measured by the interferometer and the gravity field calculated from the source mass distribution. The most critical parameters

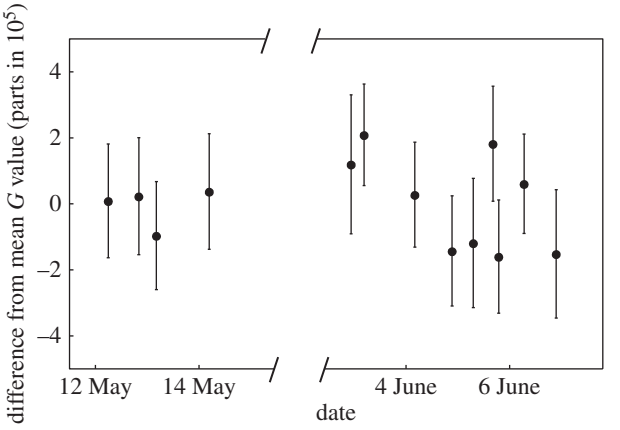

Figure 5. The predicted G values from the individual data runs taken in 2004 as the fractional deviation $\times 10^{-5}$ from the mean value of $(6.672\,34 \pm 000\,15) \times 10^{-8}$ m^3 kg^{-1} s^{-2}. The error bars include the uncertainty calculated from the data scatter within each dataset root-sum-squared with the 1.5×10^{-5} uncertainty associated with the day-to-day variations in the position measurements used in the calculation for G. The other systematic components are not included in these error bars but are included in our uncertainty in our mean G value.

in this calculation are the distances between the source mass stacks. These separations were measured daily and the G value calculated using the average distances from the measurements immediately before and after each dataset. Interferometer frequency differences and calculated G values for each set are listed in table 1, and the G values are plotted in figure 5.

Between 15 May 2004 and 3 June 2004 the motor failed and there was a significant (0.1 mm) shift in one of the source mass stacks when they hit the stops hard several times during trouble-shooting and readjustment. The gravity signal shifted by 3 parts in 10^4, but there was no significant shift in the calculated value of G after the new positions were taken into account. Between the datasets on 3 June 2004 and 4 June 2004, the source mass stacks were all rotated 180° (around their vertical axis). The scatter in the first group of points also appears lower than in the second group. This correlates with the fact that the day-to-day shifts in the measured stack positions increased by about 50% after 14 May 2004. Before we started taking data on 12 May, the source mass system had been running for some time and was well adjusted. After the motor failed, we were never able to get the system quite as well adjusted as before.

4. Interferometer design

Identical Fabry–Perot cavities and laser systems compare the displacement of the pendulum bobs with the length of the top support. The mirrors making up the cavities have a dielectric coating, which is better than 99.9% reflective at the He–Ne laser wavelength of 633 nm. The mirror surface is concave with a radius of curvature of 60 cm and the back side is flat with a single frequency antireflective coating. The length of each cavity is 34 cm corresponding to a free spectral range (FSR) of 440 MHz. The actual FSR was measured by repeatedly scanning the pendulum cavity laser from one longitudinal mode to another and the result gives (441.126 ± 0.002) MHz. This means that a 1 MHz shift in cavity frequency corresponds to a 0.72 nm change in bob separation. The fringe width was observed to be about 100 kHz, giving a finesse of approximately 4000. The laser lock is much tighter than this, with RMS noise amplitude in the upper fixed cavity less than 10 kHz in laser frequency, corresponding to a 0.007 nm mirror displacement. Most of this noise is probably due to mirror vibrations rather than actual laser noise. The noise contributed by the pendulum bob motion in the lower cavity is much larger, with an RMS amplitude of

about 200 kHz in laser frequency (corresponding to 0.14 nm in displacement) when the damping magnets were properly tuned to give an equal force on each bob. Most of this noise is at the 0.6 Hz fundamental and 5 Hz rocking modes of the pendulums. This is driven mostly by micro-seismic noise from the surrounding areas, and most of the data reported here were taken at night when it was quietest. There is also often a slow drift in the signal up to about 5 MHz h^{-1} (4 nm h^{-1}). This is consistent with the 5–10 μrad changes in floor tilt observed over the course of a typical day in our laboratory coupling into our signal through the 0.3 mm difference in pendulum length. We believe that this tilt is driven by solar heating and nightly cooling of one side of the 11-storey tower that adjoins the laboratory building. After adjusting the laser beam to match the cavity, it would remain aligned for 5–10 h before gradually drifting off the interferometer axis.

Short (11 cm long) He–Ne laser tubes were used so that only one longitudinal laser mode of each orthogonal linear polarization is supported within the 1.4 GHz wide He–Ne gain curve. The centre frequency of the pendulum bob laser was measured against an iodine-stabilized laser and found to be (473 612 400 ± 200) MHz. A heater wrapped around the laser tube provides slow (100 Hz bandwidth) frequency control of the laser. A polarizer selects one of the He–Ne polarizations. The beam then passes through a polarizing beam splitter and then an acousto-optic modulator (AOM), which provides the fast frequency control. A system of lenses, a quarter-wave plate and a mirror then retro-reflect the beam back through the AOM. This doubles the frequency shift of the AOM and more importantly cancels the frequency-dependent deflection that the AOM imparts to the laser beam. Since the beam passes through the quarter-wave plate twice, the polarization is rotated so that it now reflects off the polarizing beam splitter.

The beam now passes through a 50–50 beam splitter. One part of the beam is beat with the beam from the other cavity. The time base of the beat frequency counter was calibrated against a caesium standard and also checked against a rubidium standard several times during the experiment.

The other part of the beam proceeds through an electro-optic modulator (EOM), which imparts a phase shift that is modulated at 11 MHz. A system of lenses and a pinhole then clean up the beam and approximately match the beam divergence to the pendulum Fabry–Perot cavity. The beam then passes through another polarizing beam splitter and quarter-wave plate before it is incident on the pendulum cavity. After all the optics, only several microwatts of laser power are incident on the cavity. The light reflected from the cavity has its polarization rotated after the second pass through the quarter-wave plate and reflects off the polarizing beam splitter and falls upon a photodetector. The error signal between the laser frequency and the centre of the pendulum cavity frequency is detected using the Pound–Drever–Hall method [7]. The output of the photodetector is mixed with the EOM drive signal and fed back to the laser frequency control. The error signal is put through a double integrator and split. One path runs through a high-pass filter and is sent to the AOM control, and the other path is put through another integrator and sent to the laser tube heater control. A web-cam with the lens removed was used at the output end of the cavity during laser beam adjustment to assure that the TEM_{00} mode was excited at the start of a data run. When the source masses are moved, the pendulum bob will swing somewhat even with the magnetic damping, and occasionally this motion will cause the lasers to suddenly unlock. When this happened, only data up to the point where the laser unlocked was analysed, as it is possible that the laser would lock on a fringe other than the TEM_{00} mode.

A concern is that stray reflections between various optical elements could combine coherently to produce a systematic error in the laser signal. However, laboratory temperature variations of the order of 0.1 6°C, tilts that vary the position of the cavity mirrors with respect to the optical benches, and the constant readjustments needed to realign the optics, all cause the distance between the various optical elements to vary over the course of a run and from run to run by much more than the wavelength of the laser light. This randomizes the effects of any inadvertent Fabry–Perot cavities formed by reflections and reduces the probability of systematic errors from cavities formed by reflections off optical elements. Furthermore, for each run, we intentionally locked the laser to a different TEM_{00} fringe, so the laser frequency could vary by up to 1 GHz from run to run.

5. Pendulum design

Each pendulum bob consisted of a gold-coated oxygen-free copper cylinder with a length and outer diameter equal to 5.1 cm and an assembled mass of 780 g. A 1.9 cm bore down the centre of the bob allows the laser beam to pass through. The interferometer mirror is located within 0.1 mm of the geometrical centre of the bob. The mirror has a diameter of 2.54 cm, a thickness of 0.64 cm and a mass of 7 g. The bore on one end of the bob was widened to allow the mirror to be inserted and the removed material was then replaced with a gold-coated oxygen-free copper slip ring that was held in place with an O-ring in a groove.

The attachment for the pendulum wires was made by drilling a hole in each end of the bob 1.3 mm from the outer diameter and pressing two 2 mm (0.02 g) diameter molybdenum balls into each hole. After the balls were pressed into the holes, the drill holes were plugged with gold-coated oxygen-free copper plugs. A 0.64 mm wide slit was cut into the bob that intersected the hole 6.4 mm from the end of the bob where the two balls touched each other. This allows the pendulum wire to be slipped into the V-groove formed where the balls touch. The bobs hung from the wires, which were looped under the intersection of the two molybdenum balls to form a 'V' with the vertex at the molybdenum balls. The top of the 'V' is 73.8 cm above the centre of the bobs and 27.1 cm wide. The top of the pendulum was defined by a similar arrangement with V-grooves formed by balls pressed into holes. The pendulum wire was tungsten with a diameter of 64 μm.

In order to reduce the amplitude of the free swinging pendulums to a reasonable level, eddy current damping was required. Under each bob, two 2.5 cm diameter, 2 cm thick NdFeBr magnets were located side by side with the same poles up and mounted on a magnetic steel bar. The axis joining the two magnets was oriented perpendicular to the interferometer axis so that the field gradient experienced by the bob is large, but the net magnetization of the bob is perpendicular to the sensitive direction of the interferometer. The magnets were approximately 2 cm below the bottom edges of the bobs. To ensure that ground vibrations affected both bobs equally, the vertical height of the magnets was adjusted to minimize the noise in the cavity displacement signal and thus to match the damping force on the two bobs. With the magnets adjusted, the pendulums were slightly under-damped, with 1/e ring-down time of 2 s.

6. Source mass drive system

The drive system for the source masses was designed to be as light as possible so that most of the gravity signal came from the tungsten billets themselves. Each 120 kg stack of tungsten billets was floated on an aluminium air puck with a diameter equal to the tungsten billets and a thickness of about 2 cm. Compressed air from the building air supply at 40–60 psi was regulated down to 11–13 psi before being sent to the pucks. A groove around the outer perimeter of each air puck was connected to vacuum to sweep up the compressed air before it could escape the pucks. The pucks all rode on one large 10 cm thick piece of aluminium tool and jig plate.

The masses were moved by nylon fishing lines that formed drive belts by running around an axle on each end of the interferometer and just above the source mass stacks. An aluminium cap was epoxied to the top of each source mass stack. Attached near the perimeter of the cap on opposite sides were two clamps, which attach to a drive string. On each side of the interferometer, both source masses were attached to the same drive string and the two drive strings were looped around the same two axles to ensure that the masses all moved at the same time in order to keep the centre of mass of the configuration stationary. Also attached to the aluminium cap were three pins, which fall on either side of a rod that acts as a guide rail when the masses are in motion. The pins have a millimetre or so of clearance around the guide rail so that they did not prevent the source masses from properly locating in the stops, which define the mass positions, when they are stationary.

Each source mass stop consisted of two pillars bolted to the tool and jig source mass support plate. A disc at the top of each pillar had the rim rounded so that it contacted the centre source

mass billet at a single point half-way up the source mass stack. So the source mass location was defined by the plane of the tool and jig plate as well as the two points of contact made by each stop.

A stepper motor was attached to one of the string drive axles and was programmed to smoothly accelerate and decelerate the masses into the stops. The source masses moved the 20 cm between the stops in 35 s. Once the masses reached the stops the motor accelerated and ran for about 4 s with the drive strings slipping around the axle. This helped to ensure that the masses were firmly seated in the stops. The motor then stopped and the masses remained in place for 80 s before moving again.

The drive system was designed to be as light as possible so that it contributes as little as possible to the gravity signal. However, it would have been better to add a little additional mass in order to create a more reliable system. Since two source mass stacks were attached to each drive string, the system was over-constrained. When it was well adjusted, there was just enough elasticity in the source mass string so that both source masses on the string were firmly forced into the stops. Up until the first stepper motor failed on 15 May 2004, the system worked well. However, after the motor was replaced, stretching of the strings or the clamps slipping on the string required that the string tension be frequently adjusted. At the beginning and end of each run and about an hour into each run, we checked that the source masses were firmly registering in the stops by pressing on the source masses and verifying that there was an elastic force from the drive string pressing each mass into the stops. On several occasions the masses were found not to be registering properly during the run and the drive system was readjusted and the run restarted.

7. Dimensional measurements

The source masses for this experiment consisted of four cylindrical columns of tungsten, with each column made up of three stacked tungsten billets on an aluminium air puck and with an aluminium cap for attaching the drive string clamps and guide pins. In the inner configuration, the source masses were located on either side of the chamber, between the pendulum bob test masses. In the outer configuration, they slide alongside the chamber past the nearest bob so that the gravitational force that they exert lengthens the pendulum cavity. Each stack had a diameter of 16.6 cm, a height of 33.6 cm (the tungsten billets account for 31.1 cm of this height; each billet has a height of 10.4 cm). The transverse separation (the centre-to-centre separation of masses on opposite sides of the interferometer axis) is 26.1 cm. The longitudinal separation (the centre-to-centre separation of the source masses on the same side of the interferometer axis) is 16.7 cm in the inner position and 56.9 cm in the outer position.

The source mass configuration has the property that there are saddle points in the gravitational field that it produces. The pendulum bobs were located very near to these saddle points so that the gravitational signal from the source masses was very insensitive to the pendulum bob location. However, the signal was quite sensitive to the transverse distance between the centre of mass of the source mass pillars on opposite sides of the chamber and to a lesser extent the longitudinal distance between the centre of mass of the pillars on the same side of the chamber when the source masses are in the inner position.

To measure the transverse distance between the source masses, we constructed a large calliper out of a 10 cm thick aluminium tool and jig plate that fitted around the pendulum vacuum chamber and source masses. A schematic of this device is shown in figure 6. One side of the calliper runs on a rail and the other side was supported only at one point with a metal ball on a glass plate in order to reduce the flexing of the calliper as much as possible as it is positioned. Mechanical dial gauges were attached to each side of the calliper and used to compare the mass separations to a gauge block stack. Foam insulation was attached to the calliper where it was touched by hand in order to reduce thermal expansion effects and the reference gauge blocks were measured at both the start and end of the measurements. A similar jig was used to measure the longitudinal separations of the source masses.

The measurements with these jigs were repeated each day that gravity data were taken. The day-to-day standard deviation of the measurements is 3.6 μm (excluding 1 day where one of the

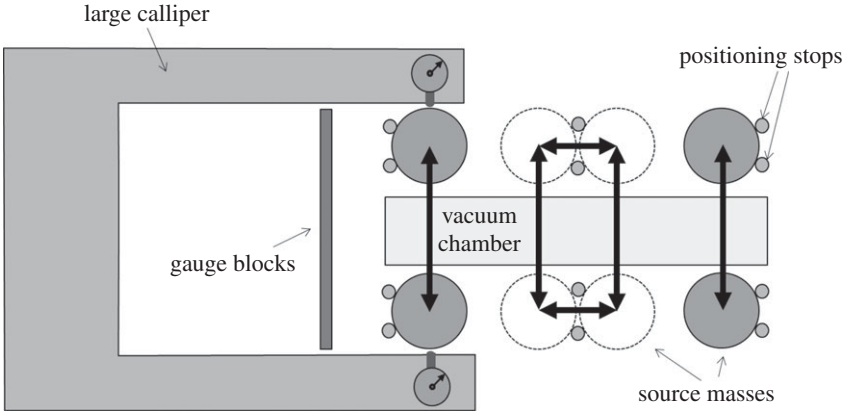

Figure 6. A schematic of the set-up used to measure the source mass separations. A top view is shown of the source masses arranged around the vacuum chamber containing the pendulum bobs in the outer position (solid lines) and in the inner position (dotted lines). The mass locations at each of these positions are defined by stops; a drive cable connected to a stepper motor is attached to the top of the source masses and moves the masses between the outer and inner positions, pulling the masses into the stops at the end of the translation. The six critical dimensions are indicated by the heavy black arrows. A calliper jig was built that fitted around the vacuum chamber and source masses. Dial indicators compared the transverse source mass separations to a stack of gauge blocks. A smaller jig, not pictured, measured the longitudinal separations of the source masses in the inner position.

source masses was accidentally run hard into a stop, resulting in a very large shift in position) and is random rather than a consistent drift in one direction. Much of this is due to actual shifts in the mass positions, since at any one time the measurements can be repeated to significantly better than 2.5 μm. For the longitudinal separation, the day-to-day standard deviation was 4.8 μm. Though this was slightly larger than the transverse variations, the calculated G value is only about a quarter as sensitive to these longitudinal position errors as it is to the transverse errors. The result of these variations should be a day-to-day fractional variation in the gravity signal of 1.5×10^{-5}, which is close to the actual standard deviation of 1.4×10^{-5} (combining the separate standard deviations of the data before and after the source masses were rotated 180°). Both the position data and the observed signal are about 50% noisier after the masses were rotated than before. This may be related to the more frequent adjustment of the source mass transport system required after the motor failed. When the gravity data were taken, the air to the pucks was always on; however, it was turned off when the position measurements were taken to ensure that the masses stay in place. As the air pucks only lift off by 3–5 μm, there was not a significant horizontal displacement in the centre of mass as the pucks settle. This was checked using an inductive sensor to measure the mass position as the air was turned on and off. This sensor was also used to verify that the source masses could be repeatably and reliably positioned in the stops.

Taking into account the scatter of the measurements, the dial indicator and gauge block accuracy, the thermal expansion of the gauge blocks and our measurement of the source mass diameter, we find an uncertainty of ±2.4 μm in the transverse separation and a ±2.6 μm uncertainty in the longitudinal separation measurements of the source masses. The uncertainty contributions from all the dimensional measurements were evaluated by repeatedly running the gravitational force integrations over the source and test mass configurations with various different parameters. The uncertainties in the longitudinal and transverse source mass separations amount to a relative uncertainty in our G value of $\pm 1.4 \times 10^{-5}$.

The gravity signal is much less sensitive to the other dimensions of the source mass distribution, but the uncertainty in these dimensions is also larger. The combined uncertainty contributions to our value of G of all these positional measurements, excluding the six critical measurements, are $\pm 0.8 \times 10^{-5}$. This includes the effect of a ±6.3 μm uncertainty location of

the top and bottom billets with respect to the centre billet in each stack. Also included is the uncertainty in the source mass to bob positions: a $\pm 50\,\mu$m uncertainty in the transverse position of the source mass centre of mass with respect to the bobs, a $\pm 80\,\mu$m uncertainty in the longitudinal position of the source mass centre of mass with respect to the bobs, and a $\pm 80\,\mu$m uncertainty in the vertical position of the source mass centre of mass with respect to the bobs.

The locations of the pendulum bobs and the source masses were referenced to the vacuum chamber bore. The location and straightness of the bore were measured with respect to the outer surfaces of the vacuum chamber. The alignment of the pendulum bobs with the bore was accomplished with a jig that slides into the chamber bore. The jig has three plates near each end of the bob, arranged with one plate on each side and one below the bob. When the bob was exactly centred in the bore, there was a $25\,\mu$m clearance between each of the plates and the bob. But if the bob makes contact with any of the plates, an electrical circuit was closed and an LED connected to that plate illuminated. Micrometer screws at the top of the pendulum allow the wire lengths to be adjusted to centre the bob in the jig. The bobs can be centred to somewhat better than $25\,\mu$m by gently setting the bob rocking and checking that the bob touches all plates equally. The pendulums were then set swinging, each with an amplitude of 1–2 cm, and a rotation stage was used to adjust each pendulum so that it did not make contact with the jig plates as it swings. A final fine rotation adjustment aligns the optical axis of the interferometer with the chamber bore. The process of wire length adjustment and rotation stage adjustment was repeated iteratively until the bob position, bob angle and pendulum translation angle were set properly. The longitudinal position of the bob in the bore was measured with a depth micrometer and an inductive sensor; the inductive sensor allows it to be seen when the micrometer makes contact and begins to move the bob.

Once the bob alignment was completed, the translation direction was checked with a telescope. Pinholes were placed at each end of the chamber precisely on the bore axis. Since the dielectric interferometer mirrors are highly reflective only near 633 nm, the broad-band light from a lamp could shine through the pinholes, allowing the telescope to be aligned with the bore axis. The pendulums were set in motion and the bobs examined through the telescope for any side-to-side motion. The angle between the bore axis and the pendulum swing was found to be (1.5 ± 0.8) mrad for one bob and (3.5 ± 1.4) mrad for the other. The angle between the optical axis of the Fabry–Perot cavity and the chamber bore was also measured to be (5.1 ± 0.7) mrad. Based on these misalignments, a correction of $(+1.7 \pm 0.4) \times 10^{-5}$ was made to the signal as read.

The only other dimensional measurement that contributes significantly to the final uncertainty are the diameters of the pendulum bobs, which have uncertainties of $\pm 2.5\,\mu$m. This contributes a fractional uncertainty of $\pm 0.1 \times 10^{-5}$ to G.

8. Mass and density of the source masses

Each source mass billet has a mass of 39.7 kg and the density variation from piece to piece is 0.04%. The fractional uncertainty in the mass of each billet is $\pm 0.6 \times 10^{-5}$. This includes the uncertainty from the air buoyancy correction of $(-12.4 \pm 0.3) \times 10^{-5}$, which takes into account the air displaced by the source masses (this is the correction to the mass measurements; the correction to our G value is of equal magnitude but opposite sign). Each stack of three billets sat on an aluminium air puck. These air pucks have the same diameter at the billets, a height of 1.9 cm and a mass of 1100 g. Each puck had two brass hose connectors (one for air and one for vacuum) and each hose connector has a mass of 1.3 g. The total mass of the plastic tubing that was dragged by each puck is approximately 2 g, though most of this mass does not move the full distance that the puck moves. Each source mass stack also has an aluminium cap, which has the same diameter as the billets, a thickness of 0.64 cm and a mass of 380 g. On each cap there were two clamps, each with a mass of 4.2 g, which attach to the drive strings and three guide pins, each with a mass of 1.0 g. The tungsten billets contain 98.7% of the total moving source mass, but since the other components are at the top and bottom of the source mass stacks and are farther away from the bobs, the billets produce 99.4% of the gravity signal. The uncertainties in the mass

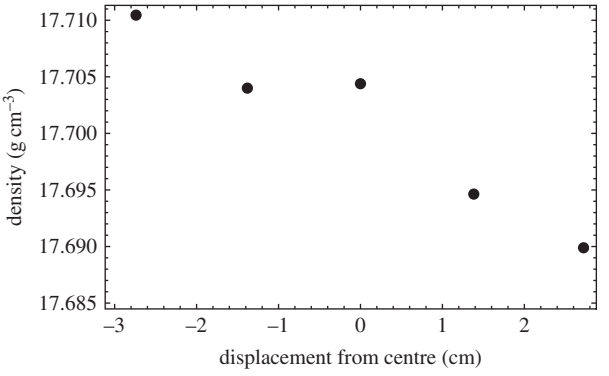

Figure 7. The density of 1 inch diameter by 1 inch high cylinders cut along a diameter of one of the tungsten billets as a function of position.

measurement of the other source mass components are not significant. The measurement of the mass of the test masses also does not contribute a significant uncertainty since this mass value appears both in the estimate of the pendulum spring constant and in the calculated gravitational force on the test mass and so cancels out to a very high degree.

These masses were used in a previous measurement of G using a free-fall gravimeter [8,9]. The source mass billets were sintered from a tungsten powder to which a binding agent of 5% (by mass) of copper and nickel were added to produce a non-magnetic alloy. The process was carried out with the billets on their side, which produced a density gradient across the billet, with the density varying by a factor of 0.001 across each billet. This density gradient was measured using an air bearing. The air bearing was machined so that it supported the tungsten source mass cylinders with the cylinder axis horizontal and so that the cylinders were free to rotate. The cylinders would naturally rotate so that the heavy side was down, and the period of oscillation around the equilibrium gives a measure of the displacement of the centre of mass from the geometric centre. For the masses used in this experiment, the period of oscillation ranged from 23 to 38 s.

The billets were arranged in the source mass stacks to cancel out the effect of the density gradient as much as possible. Based on the air bearing measurements and the arrangement of the source masses, we expect a change in the gravity signal of $(2.4 \pm 0.5) \times 10^{-5}$ if each source mass stack is rotated by 180°. When the source masses were rotated by this amount half-way through the experiment, a change of $(1.6 \pm 0.8) \times 10^{-5}$ was actually seen. The effects of a linear gradient should cancel when the average of the two orientations is taken, so no correction was applied to our G value to account for the density gradient.

As an additional check, the drive system was reconfigured to rotate the masses in place in the outer position. In this case, after correcting for small measured displacements in the mass positions as they rotated, the gravity signal changed by a factor of $(2.9 \pm 0.8) \times 10^{-5}$. Finally, sections were cut from one of the tungsten billets and do show that the density changes linearly by a factor of 0.001 across the billet. The results are shown in figure 7. Based on the variation seen here, we estimate that the contributions due to nonlinear variations in density contribute at most an error of $\pm 0.8 \times 10^{-5}$ to our G value.

9. Pendulum restoring force

The spring constant against which we are measuring our gravitational force is determined by measuring the frequency of free oscillation for each bob. Ideally, this spring constant is given by

$$k = m\omega^2, \tag{9.1}$$

where k is the spring constant, m is the bob mass and ω is the angular pendulum frequency. This k includes not only the gravitational restoring force of the pendulum, but also the elastic restoring force produced by the flexing of the wires.

The pendulum frequencies were measured in vacuum and with the damping magnets removed. For each bob, a laser beam was reflected at an angle off the back of the interferometer mirror and the return beam displacement was captured by a position-sensitive photodetector at a sampling rate of 40 Hz. The amplitude of swing was (2 ± 1) mm so that the measured frequency deviates from the zero amplitude limit by less than 2 parts in 10^6. Over several hours of measurement, the amplitude was constant to better than 2%, corresponding to a quality factor Q greater than 1×10^6, so that frequency shift due to pendulum damping is negligible. The frequencies were found to be $(0.589\,8171 \pm 0.000\,0023)$ Hz for one bob and $(0.589\,7069 \pm 0.000\,0013)$ Hz for the other, where the uncertainties come from the scatter of the data. The pendulums are quite stable, and over the course of several months the frequencies were found to be unchanged to within the measurement uncertainty of a few parts in 10^6 (the expansion coefficient of tungsten is quite low, about $5 \times 10^{-6}\,\mathrm{K}^{-1}$ at room temperature). The frequency difference between the two pendulums corresponds to a pendulum length difference of about 0.3 mm. This is not unreasonable: the pendulum bobs, themselves, were carefully aligned to within a few thousandths of an inch of nominal, but there was not a need to locate the top supports for the wires quite as accurately.

Two non-ideal effects that do need to be corrected for are the non-zero mass of the wires and the slight rotation of the bobs as they swing. The pendulum wires have a linear density of $(0.607 \pm 0.006)\,\mathrm{mg\,cm}^{-1}$. The rotational inertia of the wires modifies the pendulum frequency and introduces a correction of $(+7.54 \pm 0.08) \times 10^{-5}$ to the spring constant estimated using equation (9.1). Because of the four-wire pendulum configuration, the bobs swing with very little rotation. However, the bob centre of mass is located below the wire attachments and the loading on the front and back wires is no longer equal once the pendulum deflects. Based on both measurements of the pendulum out of the vacuum chamber, the ratio of bob rotation angle to pendulum swing angle due to differential stretching of the wires is 0.071 ± 0.005. This results in a correction to the ideal case spring constant of $(+5.9 \pm 0.4) \times 10^{-5}$ for the bob rotation.

The pendulum frequencies were measured with the pendulum damping magnets removed. However, when these magnets are in place, there will be additional forces on the bobs due to the non-zero susceptibility of the copper. This force can be found by translating the magnets and calculating the ratio of the resulting pendulum bob displacement to the original magnet displacement. In this experiment, we are directly comparing the magnetic restoring force to the pendulum spring constant and we find a correction to the pendulum spring constant of $(-7.5 \pm 0.03) \times 10^{-5}$ for one bob and $(-7.3 \pm 0.01) \times 10^{-5}$ for the other. These values are negative because the diamagnetic copper bobs moved in the opposite direction from the magnets. In addition, the damping magnets produce an upward force on the bobs, which in effect reduces g. This force was measured with a balance and found to be equivalent to a (2.6 ± 0.3) mg reduction in mass for each bob, which results in a further small correction of $(-0.033 \pm 0.004) \times 10^{-5}$ to the spring constant of each bob.

10. Tilt effects

When the source masses move, the centre of mass of the configuration moves slightly because the placement of the stops is not perfectly symmetrical. Based on the measured source mass positions, the centre of mass of the 480 kg moving source mass assembly shifts by (0.17 ± 0.05) mm along the interferometer axis for a total moment of (8300 ± 2600) g cm for the data taken from 12 May to 14 May. After 14 May, there was a change in the stop positions and the centre of mass shifted by (0.15 ± 0.05) mm for a moment of (7200 ± 2200) g cm for the 3 June to 6 June data. (The centre of mass also shifted 0.03 mm in the direction perpendicular to the interferometer axis during the 12–14 May time period and 0.003 mm in the 3–6 June time period.) Though care was taken that neither the source masses nor their support plate contact the pendulum chamber at any point, a

tilt in the source mass support plate could be transmitted to the pendulum apparatus through a tilt in the laboratory floor. To measure this effect, only the masses on one end of the apparatus were moved while the others were held stationary. This produces a torque of 4.78×10^6 g cm. Removing the calculated gravity signal from the pendulum deflection, the pendulum cavity frequency shift was found to differ from the amount expected by (-0.30 ± 0.02) MHz (out of a 62 MHz gravity signal). This corresponds to a tilt sensitivity of $(-6.3 \pm 0.4) \times 10^{-8}$ MHz g^{-1} cm^{-1}.

As an additional test, a 12 kg lead brick was placed on one end of the source mass support plate, just beyond one end of the interferometer and 43 cm from the support plate centre. The brick was then moved to a symmetrical position at the opposite end of the support plate. Since the gravity of the brick works symmetrically on the pendulum bobs, no change in the cavity length should be observed in the absence of tilt. This process was repeated several times, and the cavity length was observed to change by (0.066 ± 0.015) MHz. This gives a tilt sensitivity of $(-6.4 \pm 1.5) \times 10^{-8}$ MHz g^{-1} cm^{-1}, in good agreement with the two-mass experiment value.

Using the tilt sensitivity from the two-mass experiment, the fact that the total gravity signal is 125.4 MHz, and the moments based on the source mass position shift, we find a fractional correction to our gravity signal of $(-0.42 \pm 0.13) \times 10^{-5}$ for the 12–14 May 2004 data and a fractional correction of $(-0.36 \pm 0.11) \times 10^{-5}$ for the 3–6 June 2004 data.

11. Temperature effects

The pressure drop experienced by the air feeding the source mass air bearings raises the concern that resulting cooling could somehow influence the results, either through its effect on the damping magnets or through some other unknown mechanism. A groove around the outer edge of the pucks was connected to vacuum in order to remove the feed air before it escaped the pucks. The temperature of the source masses and support plate was measured and found to be equal to the chamber temperature to $\pm 0.1^\circ$C. The air was fed from a house air supply at 40–60 psi and then regulated down to approximately 11 psi before being fed to the puck.

To test the temperature sensitivity of the apparatus, the source masses were heated from the ambient laboratory temperature of 22°C up to 40°C. The heat was turned off and data were taken while the source masses cooled from 40°C to 30°C. During this time, the chamber reached a maximum temperature of 26°C near the source masses, and the support plate that the masses ride on reached a temperature of 28°C. Taking into account the expansion of the source mass configuration, the gravitational signal from the heated masses differed from the signal when the apparatus had completely cooled by a fractional difference of $(4 \pm 22) \times 10^{-5}$. This gives us confidence that the actual temperature gradients of less than 0.1°C across the apparatus would have a negligible effect on our results.

The experiment was conducted below ground level in a sub-basement and the room temperature was quite stable. Over the course of taking data, the laboratory temperature stayed between 21.5°C and 22.0°C.

12. Magnetic effects

The magnetization of the NdFeBr magnets has a significant temperature coefficient. Since the copper bobs are slightly diamagnetic, the damping magnets produced a small DC force on the bobs in addition to the damping force, and this could result in a temperature-driven pendulum displacement. The magnets were attached to the exterior of the vacuum chamber, but were sealed from draughts and insulated. To further reduce the temperature effect, a heater was attached to the magnets and the magnet position was adjusted so that the displacement of each bob was minimized when the temperature was changed.

It was found that, when the source masses moved through the magnetic field from the damping magnets, eddy currents were induced in the source masses, which in turn caused excessive swinging in the pendulum bobs. To reduce this effect, steel plates were placed between the chamber and the source masses in order to reduce the magnetic field at the source masses.

Even with the steel plates in place, there was some magnetic field in the region of the source masses. To check that this did not cause a problem, we deliberately placed one of the source mass stacks in a very large magnetic field. A large 5 cm diameter, 8 cm long NdFeBr magnet was placed so that the magnet pole would come within 2 mm of the mid-point of one source mass stack when the stack was in the outer position. As the source mass stack was slowing as it approached this magnet (rather than moving at full speed as it was when it was passing the damping magnets), the swinging due to induced eddy currents was not too excessive. The magnet was first located at an angle from the source mass centre parallel to the interferometer axis, and then moved around the perimeter of the stack to an angle of 60° relative to the interferometer axis. With the magnet in each position, the system was run as normal. The gravity signal varied by a factor of $(1.6 \pm 6.2) \times 10^{-5}$ between the two positions, and the mean signal with the magnets in place differed from the signal without the magnets by a factor of $(1.0 \pm 4.5) \times 10^{-5}$.

No magnetic influence was observed when the stepper motor used to move the source masses was unshielded. However, to be safe, the motor was placed inside a mu-metal box that happened to be available. When the source masses were moved, the motor would run for about 4 s after the source masses were in the stops, with the drive strings slipping around the drive shaft. This, combined with the constant adjustments required for the drive system, ensured that the angle of the motor and drive shaft was not correlated with the mass positions.

13. Gravity field modelling

The force on each bob was calculated by integrating the gravitational force over both the source mass configuration and the pendulum bobs and wires. Because the source masses are cylindrical, two of the six dimensions of this integral can be done analytically. Given a cylinder of radius R, length L and density ρ, then the radial component of the gravitational force on a point in the base plane of the cylinder and a distance a from its axis is [10]

$$F = -2G\rho \int_0^R \left\{ \ln\left(\frac{L + \sqrt{L^2 + R^2 + a^2 + 2a\sqrt{R^2 - y^2}}}{L + \sqrt{L^2 + R^2 + a^2 - 2a\sqrt{R^2 - y^2}}} \right) - \frac{1}{2} \ln\left(\frac{R^2 + a^2 + 2a\sqrt{R^2 - y^2}}{R^2 + a^2 - 2a\sqrt{R^2 - y^2}} \right) \right\} \mathrm{d}y. \tag{13.1}$$

The radial force from a cylinder at a point not in the base plane can be found by adding the force from cylinders (of positive or negative mass) with base planes that do intersect the point of interest. The gravitational field from the tungsten billets, air pucks and stack caps is calculated by numerically integrating equation (13.1). Additional point masses are added for the drive string clamps, air/vacuum hose connectors and guide pins. The resulting field is then numerically integrated over the pendulum bob body, mirror and slip ring, and the gravitational torque is integrated along the pendulum wires. The masses, dimensions and calculated gravitational fields of the source mass components are summarized in table 2.

These calculations were done using the Mathematica numerical integration function with a six-digit precision goal. These calculations were verified with a Fortran program using a Rhomberg integration algorithm to calculate the forces on the bobs for the mass positions in the first dataset. The results agree with the Mathematica results to better than one part in 10^6.

14. Summary of uncertainties

A summary of the standard uncertainty components in this experiment is given in table 3. The largest source of uncertainty is the measurement of the six-critical source mass stack separations. After this, there are a number of sources of uncertainty with a similar magnitude. These include the other dimensional measurements as well as density variations in the source masses that are not compensated for by rotating the source mass stacks. The uncertainty in the pendulum spring constants includes both the measurement of the frequency of oscillation of the pendulums

Table 2. The source mass model of one stack and the magnitude of the component, along the interferometer axis, of the resulting gravitational acceleration. The acceleration is given in μGal, where 1 μGal = 10^{-8} m s^{-2}.

part	modelled as	mass (g)	dimensions (cm)	x, y, z location[a] (cm)	gravity signal[b] (μGal)
centre tungsten billet	cylinder	39 700[c]	height = 10.4[c]	$x = 28.4/8.3$[f]	
			diam. = 16.6[c]	$y = 13.1$[f]	14
				$z = -0.2$[g]	
top tungsten billet	cylinder	39 700[c]	height = 10.4[c]	$x = 28.4/8.3$[f]	
			diam. = 16.6[c]	$y = 13.1$[f]	8.6
				$z = 10.1$[g]	
bottom tungsten billet	cylinder	39 700[c]	height = 10.4[c]	$x = 28.4/8.3$[f]	
			diam. = 16.6[c]	$y = 13.1$[f]	8.3
				$z = -10.6$[g]	
air puck	cylinder	1105[c]	height = 1.9[c]	$x = 28.4/8.3$[g]	
			diam. = 16.6[e]	$y = 13.1$[g]	0.099
				$z = -16.7$[g]	
stack cap	cylinder	376[c]	height = 1.9[e]	$x = 28.4/8.3$[g]	
			diam. = 16.6[e]	$y = 13.1$[g]	0.048
				$z = 15.6$[g]	
drive string clamp no. 1	point	4.1[d]		$x = 36.0/15.9$[g]	
				$y = 13.1$[g]	
				$z = 16.3$[g]	
drive string clamp no. 2	point	4.1[d]		$x = 26.7/0.6$[g]	
				$y = 13.1$[g]	
				$z = 16.3$[g]	
air/vacuum hose connector no. 1	point	1.3[d]		$x = 29.2/9.1$[g]	
				$y = 21.4$[g]	
				$z = -16.7$[g]	
air/vacuum hose connector no. 2	point	1.3[d]		$x = 27.6/7.5$[g]	
				$y = 21.4$[g]	0.001[i]
				$z = -16.7$[g]	
cap guide pin no. 1	point	1.1[d]		$x = 22.2/2.1$[g]	
				$y = 17.7$ and 8.5[g,h]	
				$z = 16.4$[g]	
cap guide pin no. 2	point	1.1[d]		$x = 34.5/14.4$[g]	
				$y = 17.7$ and 8.5[g,h]	
				$z = 16.4$[g]	
cap guide pin no. 3	point	1.1[d]		$x = 28.4/8.3$[g]	
				$y = 20.9$ and 5.3[g,h]	
				$z = 16.4$[g]	

(*Continued*.)

Table 2. (*Continued.*)

[a]Coordinate origin is the point half-way between the pendulum bobs. The *x*-axis is along the interferometer axis and the *z*-axis is vertical. Two *x*-coordinates are given for each part corresponding to the inner and outer source mass positions.
[b]The gravity signal is calculated by taking the difference in accelerations at the two pendulum bobs and then taking the difference in this value between the inner and outer source mass positions. This is the signal from only one of the four source mass stacks.
[c]The exact value for this parameter is measured for each part.
[d]All parts of this type were weighed together, and the value for each part of this type is taken to be the average weight.
[e]The value for this parameter is taken to be the same for all parts of this type.
[f]The exact value for this position was recalculated each day.
[g]The value for this parameter was different for each stack, but for each stack it was taken to be constant during the experiment.
[h]The two values for this coordinate are before and after the stacks were rotated 180°. (Only the cap pins rotated. The air/vacuum hose connectors were moved so that they remained on the side of the stack opposite the pendulum chamber when the stacks were rotated.)
[i]This is the total gravity signal from all point masses.

Table 3. A summary of the uncertainty budget.

	fractional uncertainty contribution to G ($\times 10^{-5}$)
six critical source mass dimensional measurements	1.4
all other dimensional measurements	0.8
density variations within the source mass billets	0.8
pendulum spring constants	0.7
mass measurement	0.6
interferometer	0.6
scatter of the 11 gravity measurements	0.4
tilt effects due to the source mass motion	0.1
combined uncertainty	2.1

as well as the uncertainties in the corrections to the spring constant due to non-ideal effects. The mass measurement uncertainty includes both the uncertainty in the scale used to weigh the masses as well as the uncertainty in the air buoyancy correction. The uncertainty in the interferometer component includes the scatter of the FSR measurements as well as uncertainties due to the alignment of the optical axis and bob translation directions with respect to the rest of the apparatus. There are smaller uncertainty components due to the scatter of the gravity data as well as an uncertainty in our tilt correction. The root-sum-square combination of these uncertainty components is 2.1 parts in 10^5.

Acknowledgements. We thank Hans Green, Blain Horner and Alan Patee of the JILA instrument shop for creating this beautiful apparatus. We also thank Douglas S. Robertson for writing the Fortran code used to check our gravity field calculations, as well as Terry Quinn and Richard Davis for many helpful discussions.
Funding statement. H.V.P. is grateful to the National Research Council for an NIST post-doctoral fellowship. Sandia National Laboratories is a multiprogramme laboratory operated by Sandia Corporation, a wholly owned subsidiary of Lockheed Martin Company, for the US Department of Energy's National Nuclear Security Administration under contract DE-AC04-94AL85000.

References

1. Parks HV, Faller JE. 2010 Simple pendulum determination of the gravitational constant. *Phys. Rev. Lett*. **105**, 110801. (doi:10.1103/PhysRevLett.105.110801)
2. Mohr PJ, Taylor BN, Newell DB. 2012 CODATA recommended values of the fundamental physical constants: 2010. *Rev. Mod. Phys.* **84**, 1527–1605. (doi:10.1103/RevModPhys.84.1527)

3. Cohen ER, Taylor BN. 1987 The 1986 adjustment of the fundamental physical constants. *Rev. Mod. Phys.* **59**, 1121–1148. (doi:10.1103/RevModPhys.59.1121)
4. Schurr J, Klien N, Meyer H, Piel H, Walesch H. 1991 A new method for testing Newton's gravitational law. *Metrologia* **28**, 397–404. (doi:10.1088/0026-1394/28/5/004)
5. Walesch H, Meyer H, Piel H and Schurr J. 1995 The gravitational force at mass separations from 0.6 m to 2.1 m and the precise measurement of G. *IEEE Trans. Instrum. Meas.* **44**, 491–493. (doi:10.1109/19.377889)
6. Kleinevoß U, Meyer H, Schumacher A, Hartmann S. 1999 Absolute measurement of the Newtonian force and a determination of *G. Meas. Sci. Tech.* **10**, 492–494. (doi:10.1088/0957-0233/10/6/313)
7. Black ED. 2001 An introduction to Pound–Drever–Hall laser frequency stabilization. *Am. J. Phys.* **69**, 79–87. (doi:10.1119/1.1286663)
8. Schwarz PJ. 1998 The free-fall determination of the universal constant of gravity. PhD thesis, University of Colorado Boulder, Boulder, CO, USA.
9. Schwarz JP, Robertson DS, Niebauer TM, Faller JE. 1998 A free-fall determination of the Newtonian constant of gravity. *Science* **282**, 2230–2234. (doi:10.1126/science.282.5397.2230)
10. Chen YT, Cook A. 1993 *Gravitational experiments in the laboratory*, ch. 6.3. Cambridge, UK: Cambridge University Press.